Effects of thermal and mechanical deformations on textured thrust bearings optimally designed by a THD calculation method

Michail Chalkiopoulos, Anastasios Charitopoulos, Michel Fillon, Christos Papadopoulos

Effects of thermal and mechanical deformations on textured thrust bearings optimally designed by a THD calculation method

Michail Chalkiopoulos [b], Anastassios Charitopoulos [a,b,*], Michel Fillon [a], Christos I. Papadopoulos [b]
*anastasios.charitopoulos@univ-poitiers.fr
[a]Institut Pprime, CNRS - University of Poitiers -ISAE- ENSMA, Dpt GMSC, Futuroscope Chasseneuil, France
[b]School of Naval Architecture and Marine Engineering, NTUA, Zografos, Greece

Abstract. A performance optimisation study of a thrust bearing with surface texturing has been addressed. Bearing response calculations have been performed with a thermohydrodynamic modelling approach. A THD-optimal bearing design has been calculated, and a sensitivity analysis has been performed. The optimal design has been evaluated utilising a thermoelastohydrodynamic model, in order to quantify the effects of thermal deformations on tribological characteristics, and a sensitivity analysis demonstrated a small difference on the parameter set of the optimal geometry. However, bearing performance is substantially affected by thermal deformations, leading to a reduction of thrust load by 13% and an increase of friction coefficient by 10%. The presented results highlight the importance of modelling thermal deformation on the design of textured thrust bearings.

Keywords: Parallel surface thrust bearings; Surface texturing; Optimisation; TEHD regime;

INTRODUCTION

Many studies have been conducted aiming at optimising texture design and evaluating the effects of texturing on the tribological characteristics of thrust bearings [1-3]. In most of the studies, the conclusion drawn was that, for each application, the optimal texture parameters differ (in terms of texture region, shape, and depth), thus individual studies need to be performed on a per-case basis [4]. Moreover, the optimised texture parameters have shown to improve the performance characteristics of the bearings in a narrow range of operating conditions, but both computational [5] and experimental studies [6] have pointed out that, for high values of specific pressure, the positive effect of textures decreases dramatically, whereas, in some conditions, even a plain parallel thrust bearing exhibits better tribological characteristics than a partially textured thrust bearing optimised for different operating conditions [6-7]. At high values of specific pressure, mechanical and/or thermal deformations of the bearing geometry become significant, therefore more advanced modelling procedures are required, in order to evaluate the optimal texture geometry of the bearings [8-17].

The present study consists of two parts. The first part is to identify an optimal textured parallel thrust bearing geometry, for given operating conditions, utilising the state-of-the-art approach from the current literature [18-21]. Thus, a 3D CFD approach has been selected. A thermo-hydrodynamic (THD) model has been generated, considering viscous dissipation, solution of the energy equation in the fluid domain, and conjugate heat transfer in the solid domains. An optimisation problem has been defined, with two objective functions, namely the load carrying capacity (LCC) and the friction torque. The sector pad thrust bearing geometry modeled in the present study is a parallel thrust bearing featuring a 6 by 4 array of rectangular dimples at the inflow region of the bearing pad, in the circumferential and radial directions, respectively. The optimisation parameters of texture geometry are (a) the textured length, as a percentage of the total pad angle, (b) the textured width, as a percentage of the total pad width, and (c) the textured depth, in microns. A genetic algorithm optimisation procedure has been utilised, following the work of Papadopoulos et al. [22]. After the optimisation has been concluded, a parametric analysis has been performed in a narrow

range of the optimised parameters, in order to verify that the optimised geometry is indeed the global optimum. In the second part of the present study, a thermo-elasto-hydrodynamic (TEHD) [23-25] model has been generated, taking into consideration the mechanical and thermal deformation of the pad domain. The THD optimised geometry has been re-evaluated with the TEHD modelling approach. Moreover, a second parametric analysis has been performed, in order to identify, with the more advanced TEHD modelling approach, that the previous identified optimum is in fact the optimum while the thrust bearing operates highly loaded. Finally, the bearing performance parameters in TEHD conditions have been evaluated and compared to those corresponding to THD.

The main goal of the present study is not to optimise the texture slider bearing, but in the contrary to identify why in real applications the textured configuration exhibits worst tribological characteristics, and why that the contemporary calculation methods overestimate its performance capabilities.

NUMERICAL MODEL

Basic Geometry

Three different domains make up the present computational model, namely the pad, the fluid, and the rotor, depicted in Fig. 1. The thrust bearing geometry selected for the present study, is the one presented by the experimental work of Henry et al. [6]. All operating conditions have been set in accordance with the aforementioned work. The dimensions of the thrust bearing can be displayed in Table 1. The gap between the rotor and the stator constitutes the lubricant domain. In order to be able to take into account the oil mixing, the groove geometry needed to be modelled. Thus, half of the fore and aft grooves have been incorporated in the geometry of the sector pad model. Including the groove geometry, helps for the more accurate representation of the hot-oil-carry-over phenomenon.

Table 1– Basic dimensions of the thrust bearing model.

Dimension	Value	Units
Pad Angle (L)	45	deg
Pad Width (B)	20	mm
Pad Thickness	10	mm
Rotor Thickness	20	mm
Groove Length	3	mm
Groove Depth	4	mm
Inner Diameter	50	mm
Outer Diameter	90	mm

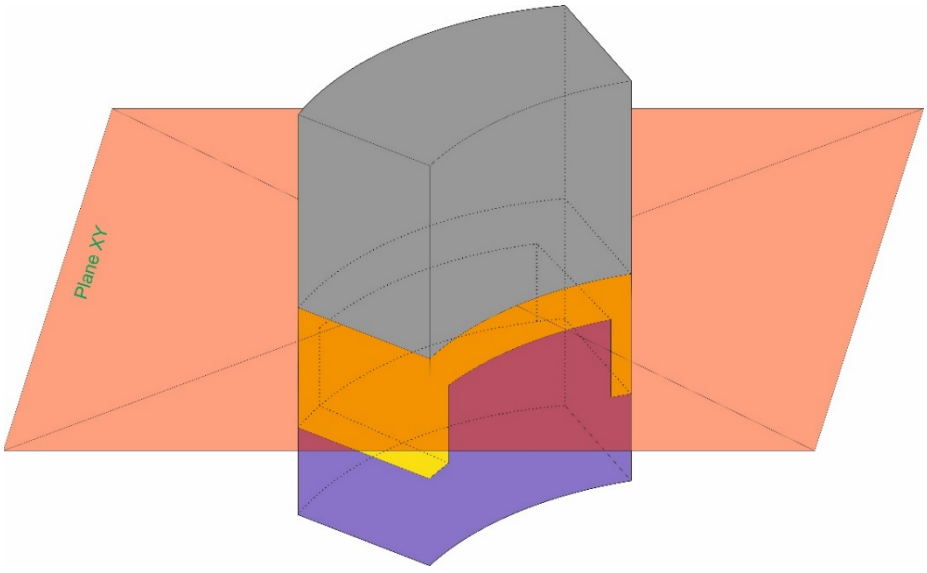

Figure 1– Calculation domains of the sector pad thrust bearing.

Texture Geometry Parameters

The designed textured geometry consists of 24 rectangular, 6 dimples in the circumferential direction and 4 dimples in the radial direction with a texture density ρ of 80%. Schematic of the texture configuration is presented in Fig. 2. The overall textured width is calculated as a percentage of the total pad width and the textured length as a percentage of the total pad angle, excluding the grooves. The textured depth is constant for all the dimples; in the present study it is varied between 10 μm and 50 μm.

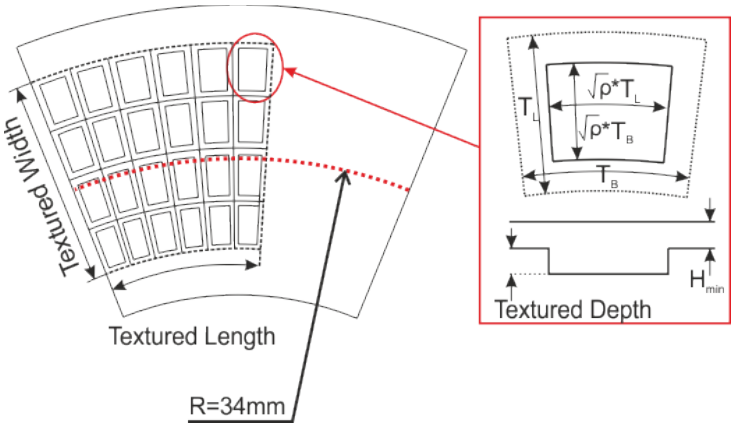

Figure 2- Optimisation parameters of the textured geometry.

Meshing procedure

The mesh of the THD and TEHD models is identical. A detailed mesh study has been conducted, in order to evaluate the final mesh parameters. For all three domains a structured mesh has been generated, with 150 elements in the circumferential direction, and 60 in the radial. Namely the total number of elements for the three domains are: a) for the pad 910,000 elements, b) for the lubricant 340,000, with 15 layers of hexahedral elements in the cross-flow direction and 15 layers in the cross-flow direction inside the textured area, c) for the rotor 350,000 elements. The elements utilised in this study are the Solid 226 elements for the Pad geometry, and HEXA_8 for the fluid and rotor domain. In Fig. 3 a visual representation of the utilised mesh is presented. Mesh and convergence studies have been performed previously [26], and the same parameters have been utilised.

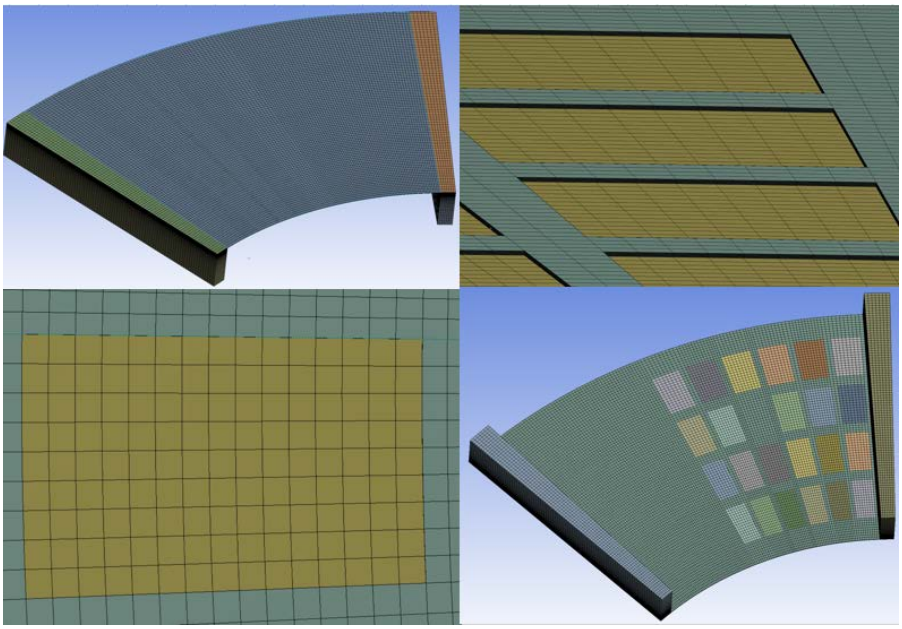

Figure 3- Mesh details

Boundary Conditions

The fluid surrounds the thrust bearing; thus, the pad is considered fully flooded. Inlet pressure of 1 bar is imposed on the fluid inner surface, as denoted in Fig. 4. Following the work in [5], the heat transfer coefficients and temperatures have been considered accordingly, to both solid domains, see Fig. 4 and Table 2. The inner surface of the bearing pad is in contact with oil, the outer surface is in contact with air, and the bottom surface is in contact with steel (shaft), therefore, appropriate values of heat transfer coefficients have been selected at each location (more details can be found in reference [26]). The same procedure has been followed to account for the heat transfer coefficients of the rotor surfaces.

The bottom surface of the pad domain has been considered fixed. The rotor domain has been considered rigid. The thermophysical properties of both solid domains' material are introduced in Table 3. The thermophysical properties of the lubricant are introduced in Table 4. The ISO VG 46 lubricant has been utilised, with a constant density of 870 kg/m^3, and a temperature dependent viscosity. The viscosity has been modeled according to the McCoull and Walther relation [5]:

$$log(log(v + a)\,) = b - nlog(T)$$

where, ν is the kinematic viscosity (cSt), T is the temperature and a = 0.6, b = 9.02865, and n = 3.52681. Finally, the rotational speed of the rotor for all the calculations of the present study has been set at 6000 RPM, the resulting sliding velocity in the mid-radius of the bearing is approximately 22 m/s.

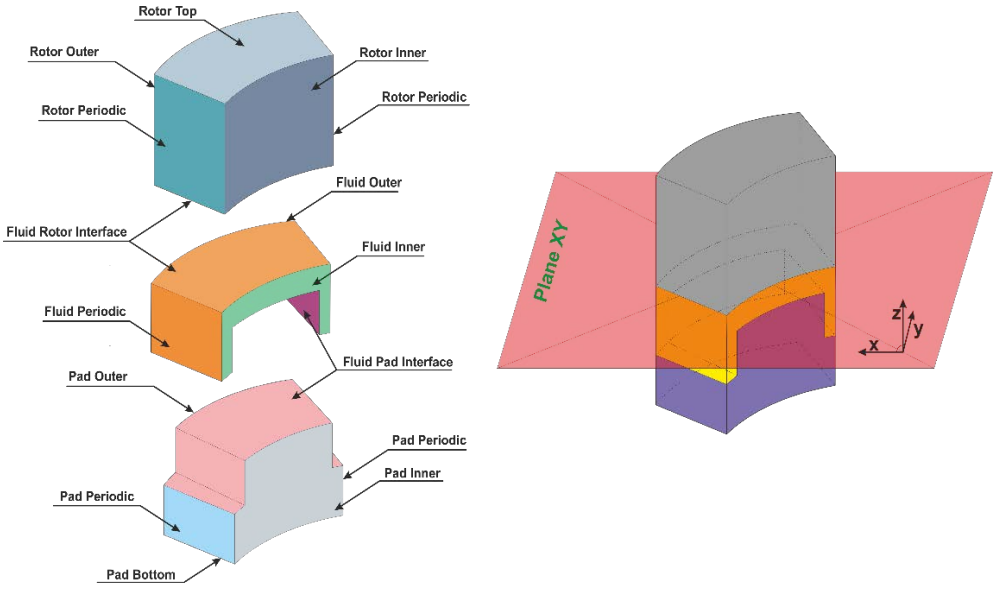

Figure 4 - Computational model: designation of domain surfaces.

Table 2 - Boundary conditions of the models.

Pad		
Top surface	Fluid-Solid interface: Continuity of heat flux and temperature	Free displacement in all directions
Bottom surface	Heat transfer coefficient: 1000 W/(m^2.K), T=40 °C	Fixed
Inner surface	Heat transfer coefficient: 200 W/(m^2.K), T=40 °C	Free displacement in all directions
Outer surface	Heat transfer coefficient: 25 W/(m^2.K), T=40 °C	Free displacement in all directions
Sides	Periodic conditions	Free displacement on the surface plane
Rotor		
Top surface	Heat transfer coefficient: 25 W/(m^2.K), T=20 °C	Fixed
Bottom surface	Fluid-Solid interface: Continuity of heat flux and temperature	Fixed
Inner surface	Heat transfer coefficient: 1000 W/(m^2.K), T=20 °C	Fixed
Outer surface	Heat transfer coefficient: 25 W/(m^2.), T=20 °C	Fixed
Sides	Periodic conditions	Fixed
Fluid		
Fluid/Rotor interface	Fluid-Solid interface: Continuity of heat flux and temperature	Fixed
Fluid/Pad interface	Fluid-Solid interface: Continuity of heat flux and temperature	Free displacement in all directions
Fluid Sides	Periodic conditions	Free displacement on the surface plane
Fluid Inner surface	Opening with temperature 40 °C and static relative pressure 1 bar	Free displacement in z direction
Fluid Outer surface	Opening with temperature 20 °C and static relative pressure 0 bar	Free displacement in z direction

Table 3 - Thermophysical properties of the pad and rotor materials.

Property	**Rotor/Pad (Steel)**	**Units**
Specific Heat Capacity	434	J/(kg.K)
Thermal Conductivity	60.5	W/(m.K)
Molar Mass	55.85	kg/kmol
Density	7854	kg/m^3
Thermal Expansion Coef.	$1.2x10^{-5}$	C^{-1}
Young's Modulus	215	GPa

Table 4 - Thermophysical oil properties.

ISO VG 46 Oil Parameters			
Symbol	Value	Units	Comments
ρ	870	kg m^3	Oil density
c	2.1	kJ (kg.K)	Specific heat capacity
k	0.13	W/(m.K)	Thermal conductivity

TEHD modelling procedure

The thermoelastohydrodynamic (TEHD) model has been generated utilising a commercial code (Ansys CFX and Ansys Mechanical). A 2-way FSI modelling approach has been utilised for the fluid/pad interface, where the CFX and FE solvers exchange data for the continuity of the temperature and pressure on both domains. In particular, (a) temperature and pressure field data are transferred from the CFD to the FE solver, and (b) mesh displacement and heat flux of the interface from the FE to the CFD solver. The bearing pad geometry can deform due to (i) the temperature gradient, and (ii) pressure generated within the thin lubricant film.

For the solution of the TEHD model, the below presented steps have been followed:

- The Finite Element solver evaluates the thermal expansion of the pad domain, for an initial temperature difference of twenty degrees Celsius. Then the transformed geometry is transferred to the CFD solver.
- In the second step the flow of the lubricant domain is calculated. This includes the solution of the conjugate heat transfer in the rotor domain.
- The calculated temperature and pressure profile of the fluid/pad interface are transferred to the Finite Element solver in order to re-evaluate the mesh displacement due to thermal and mechanical deformation on the pad domain.
- This procedure iterates until the difference of the maximum nodal displacement of two consecutive steps is less than a preset value.
- In the final step, all the tribological characteristics of the bearing are evaluated.

In order to evaluate the bearing performance on a specific minimum film thickness, five values of the initial minimum thickness of the fluid domain are selected and evaluated. The resulting minimum film thickness values are plotted versus the initial minimum film thickness, and by interpolating with a polynomial equation, the required initial minimum film thickness is evaluated. Finally, the model is recalculated in order to acquire the performance of the bearing with the wanted final minimum film thickness.

The algorithm utilised for calculating the bearing characteristics is depicted in Fig. 5. The computational time needed for the above modelling approach is approximately 5 days in a 24-core computer, for a single minimum film thickness evaluation. In comparison a simple THD model needs only 3hours on the same computer.

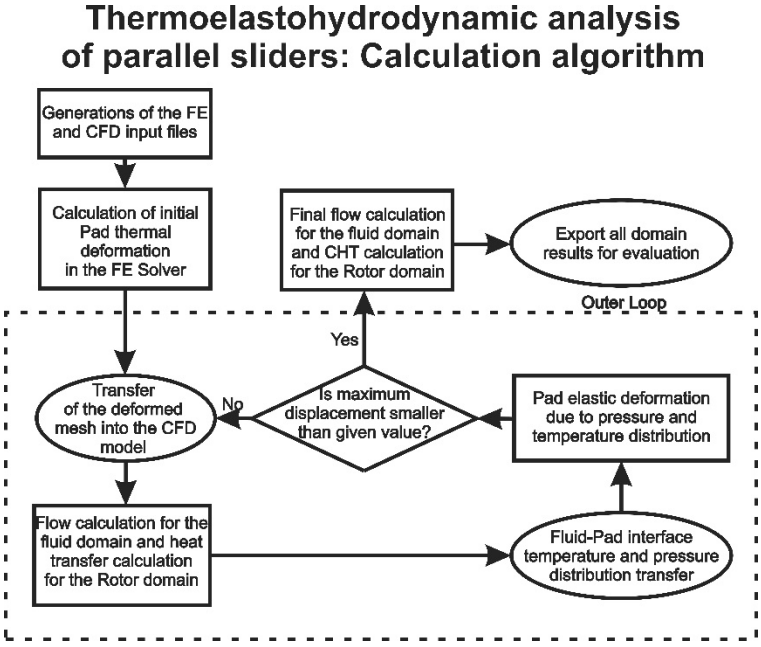

Figure 5- ThermoElastoHydroDynamic analysis of parallel thrust bearings: Calculation algorithm.

Governing equations

All equations have been solved utilising the commercial codes ANSYS CFX and ANSYS MECHANICAL [28]. The above codes have been validated multiple times in the literature with experimental date [29].

The equations solved are presented below:

Mass conservation equation: $\nabla \cdot V = 0$ [1]

Momentum equations: $\rho(V\Delta)V = -\nabla p + \nabla \cdot (\mu \cdot \nabla V)$ [2]

Energy equation, fluid domain: $\rho \cdot c_{pf} \cdot v \cdot \nabla T = \nabla\left(\lambda_f \cdot \nabla T\right) + \mu\Phi$ [3]

Energy equation, solid domains: $\nabla(\lambda_s \cdot \nabla T) = 0$ [4]

The pad undergoes elastic deformation due to (a) pressure distribution on the fluid/pad interface, and (b) the thermal expansion of the solid. The stress is related to strain by:

$$\{\sigma\} = [D] \cdot \{\varepsilon^{el}\} \quad [5]$$

where $\{\varepsilon^{el}\} = \{\varepsilon\} - \{\varepsilon^{th}\}$, and $\{\varepsilon^{th}\} = [a^{se}, a^{se}, a^{se}, 0,0,0]^T$ [6]

where α^{se} represents the coefficient of thermal expansion.

The cavitation model utilised is the Rayleigh Plesset described by the equation [7].

$$R_B \frac{d^2R_B}{dt^2} + \frac{3}{2}\left(\frac{dR_B}{dt}\right)^2 + \frac{2\sigma_B}{\rho R_B} = \frac{p_v - p}{\rho} \quad [7]$$

where R_B is the bubble radius, p_v is the pressure inside the bubble (the vapor pressure is calculated at the temperature of the surrounding lubricant), p is the pressure in the liquid surrounding the bubble, ρ is the liquid density, and σ_B is the surface tension coefficient between the liquid and vapor. No thermal barriers are considered between the liquid and the vapor.

The calculation of the load carrying capacity (*LCC*) of the thrust bearing is evaluated on the fluid/rotor (*FSI*) interface by the following expression [8]:

$$LCC = \iint_{FSI} p(x,y)\, dx\, dy \quad [8]$$

The friction torque (*Fr*) is evaluated on the fluid/rotor interface.

RESULTS

THD Optimisation

The THD model optimisation results are depicted in Fig 6. The red points correspond to the Pareto optimal designs, whereas the blue points account for all the calculated intestines of the parametric model. As it can be observed from Fig. 6, no specific congestion points have been identified. The optimal design parameters that have been selected for the present study are those of the Pareto point with the smallest coefficient of friction, which is also the one with the largest value of LCC. In Table 5, the selected parameter set is presented.

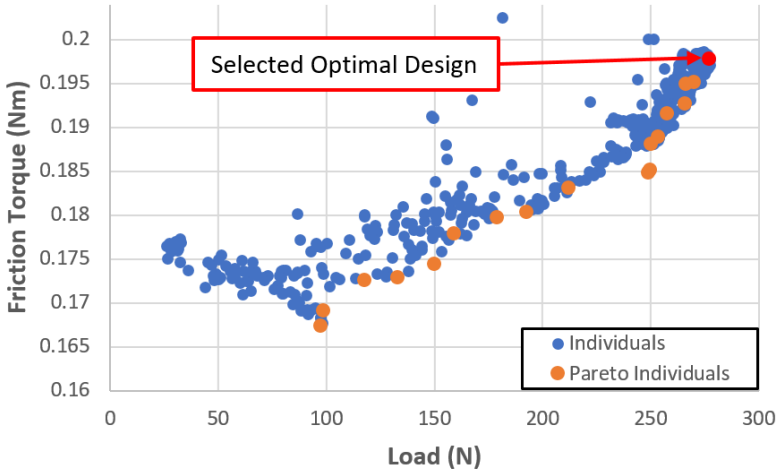

Figure 6 – Optimisation Pareto front.

Table 5 – Selected Optimal Design Parameters

Selected Optimal Parameter Set	
Texture Length	56.20%
Texture Width	84.70%
Textured Depth	23 μm
Objective Function Values	
Load Carrying Capacity	278.2 N
Friction Torque	0.198 Nm
Coefficient of Friction	0.0203
Inlet Flow Rate / Pad	0.1 l/min

The resulting pressure field of the THD optimal configuration is illustrated in Fig. 7a. The maximum oil pressure has been calculated at 1.75 *MPa*, resulting in an overall LCC of 278.2 *N*, a friction torque of 0.198 Nm and a coefficient of friction of 0.0203. On the second dimple of the outer radius, a pressure drop occurs, therefore a cavitating region has been created, as seen in Fig. 7b. The maximum oil temperature has been calculated at 92.7 ℃ at the midline of the film thickness as displayed in Fig. 7d. At the fluid/pad and fluid/rotor interfaces the temperature is higher at the outer radius region of the trailing edge, as seen in Fig. 7c and Fig. 7e. The oil entering the pad is heated due to shear stresses, and the centrifugal forces force the hot oil to move at the outer radius region of the trailing edge. The temperature of the rotor is significantly higher compared to that of the stator in Fig. 7f. The calculated results are presented on Table 6.

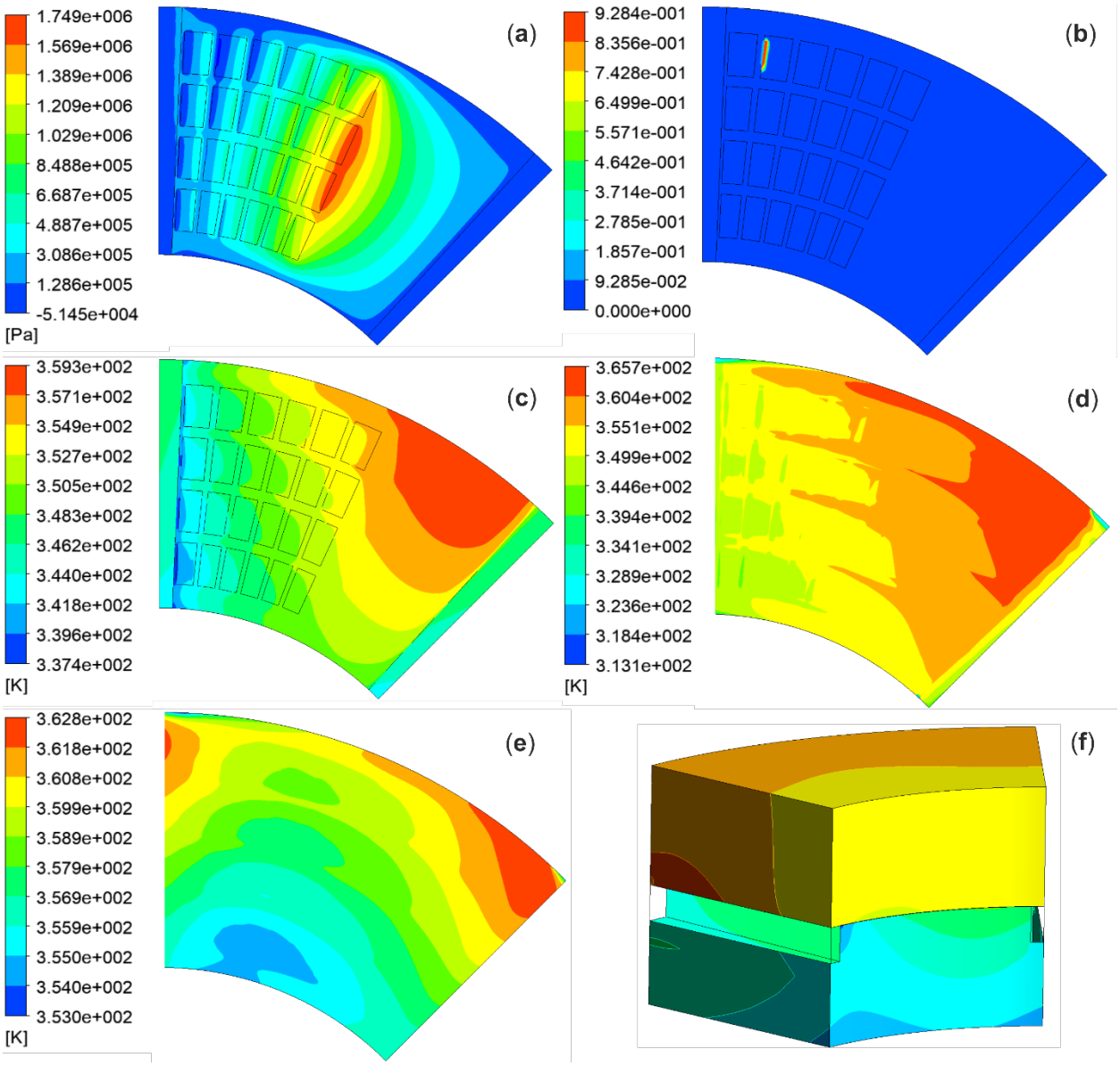

Figure 7 – (a) Pressure field at the fluid/pad interface, (b) Volume fraction field (blue: liquid oil, red: oil vapor) at the fluid/pad interface, Temperature field at (c) fluid/pad interface, (d) midplane of Film Thickness, (e) fluid/rotor interface, (f) pad and rotor outer surfaces.

Table 6 – THD Optimal Design Results

Min. Film Thickness	20 μm
Max Oil Pressure	1.75 MPa
Load Carrying Capacity	278.2 N
Friction Torque	0.198 Nm
Coefficient of Friction	0.0203
Max Oil Temperature	92.7 °C
Max Air/Oil Vol. Fraction	92.80%

THD Sensitivity Analysis

In the vicinity of the optimal parameter set, a parametric analysis has been conducted, in order to identify the sensitivity of the design parameters. For the textured Length (L) and textured Width (B) limits of ±5% of the optimal value have been considered and for the textured Depth (TD) limits of ±3μm. As shown in Fig. 8 the local optimality is validated. Although for some parameter values the friction torque seems lower than the optimal, the LCC is also substantially decreased leading to a higher COF.

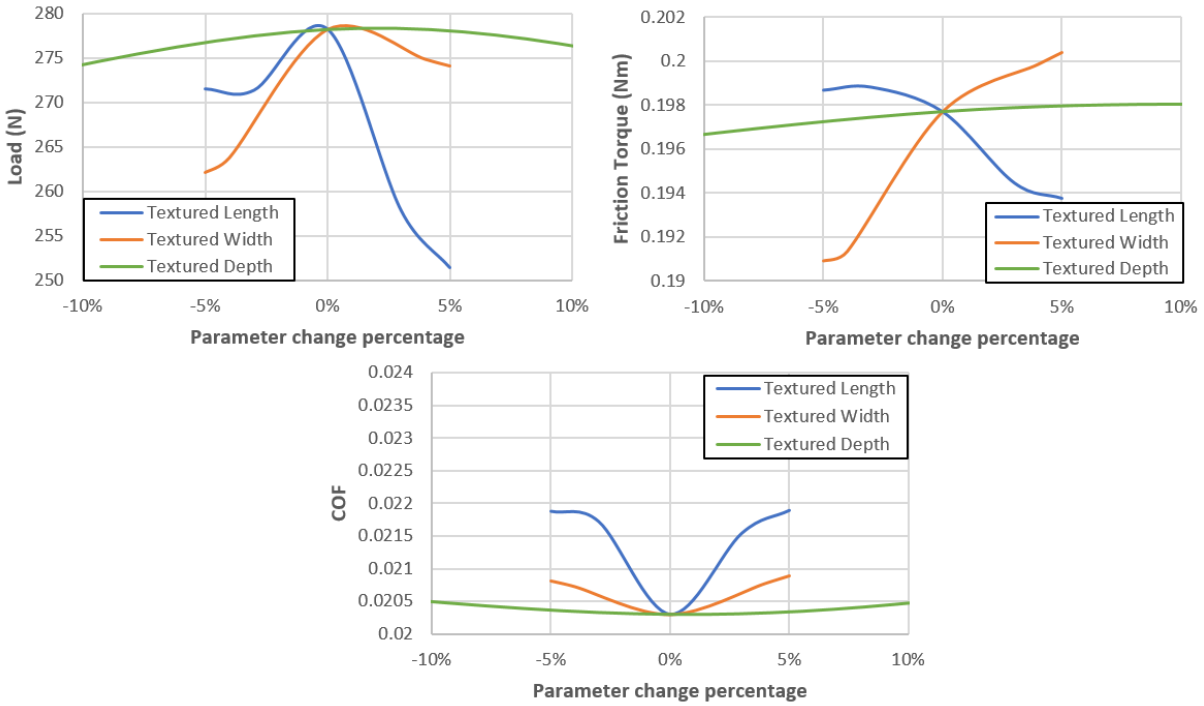

Figure 8 – THD Parametric analysis a) LCC, b) Friction torque c) Friction coefficient.

Re-evaluation of the THD-optimal design using TEHD analysis. Comparison of THD and TEHD simulation results

The optimal THD design has been re-evaluated using the TEHD based analysis. The results shown on Fig. 9a indicate a substantial alteration of the fluid/pad interface geometry due to the thermal and mechanical deformation of the pad domain. The deformed geometry affects significantly all the fields resulting in a decreased LCC and an increase of the coefficient of friction. The main evaluation results are presented on Table 7.

Table 7 – TEHD evaluation results

Min. Film Thickness	20 μm
Max Oil Pressure	1.72 MPa
Load Carrying Capacity	242.6 N
Friction Torque	0.190 Nm
Coefficient of Friction	0.0224
Max Oil Temperature	89.5°C
Max Air/Oil Vol. Fraction	63.50%
Maximum Mesh Displacement	9.7 μm

The mechanical and thermal deformation on the vertical axis leads to the formation of a converging region, which extends from the leading edge of the pad (inflow) to the end of the textured surface area, and a diverging region, from the end of the textured surface area to the trailing edge (outflow). The converging region results in a more efficient pressure build up in the inflow direction, due to the synergetic effect of the converging wedge and the dimple geometry. This increased pressure build-up eliminates the cavitation into the dimples, present in the THD simulations. However, because of the diverging geometry in the outflow region, the pressure drop gradient is substantially increased, therefore a cavitating region is created on the outer radius of the trailing edge as observed in Fig.9c. The pressure-drop combined with the lower maximum pressure decreases the load carrying capacity of the bearing. The difference on the pressure and cavitation fields of THD and TEHD models is indicated on Fig.7 and Fig. 9, while the final geometry of the lubricant film can be clearly observed in Fig.10. Focusing on Fig. 11, we may observe that from 0° to 22.5° of the bearing, the pressure build-up of the TEHD model is slightly increased. However, from 24.5° to 45° the pressure drops sharply for the TEHD model, leading to a decreased overall pressure integral and therefore a lower value of load carrying capacity. Moreover, the overall oil temperature is lower for the TEHD model as pointed out in Fig. 12. This can be attributed to the insertion of more cold fluid into the pad domain due to the converging region in the inlet. The difference of the calculated values can be seen in table 8.

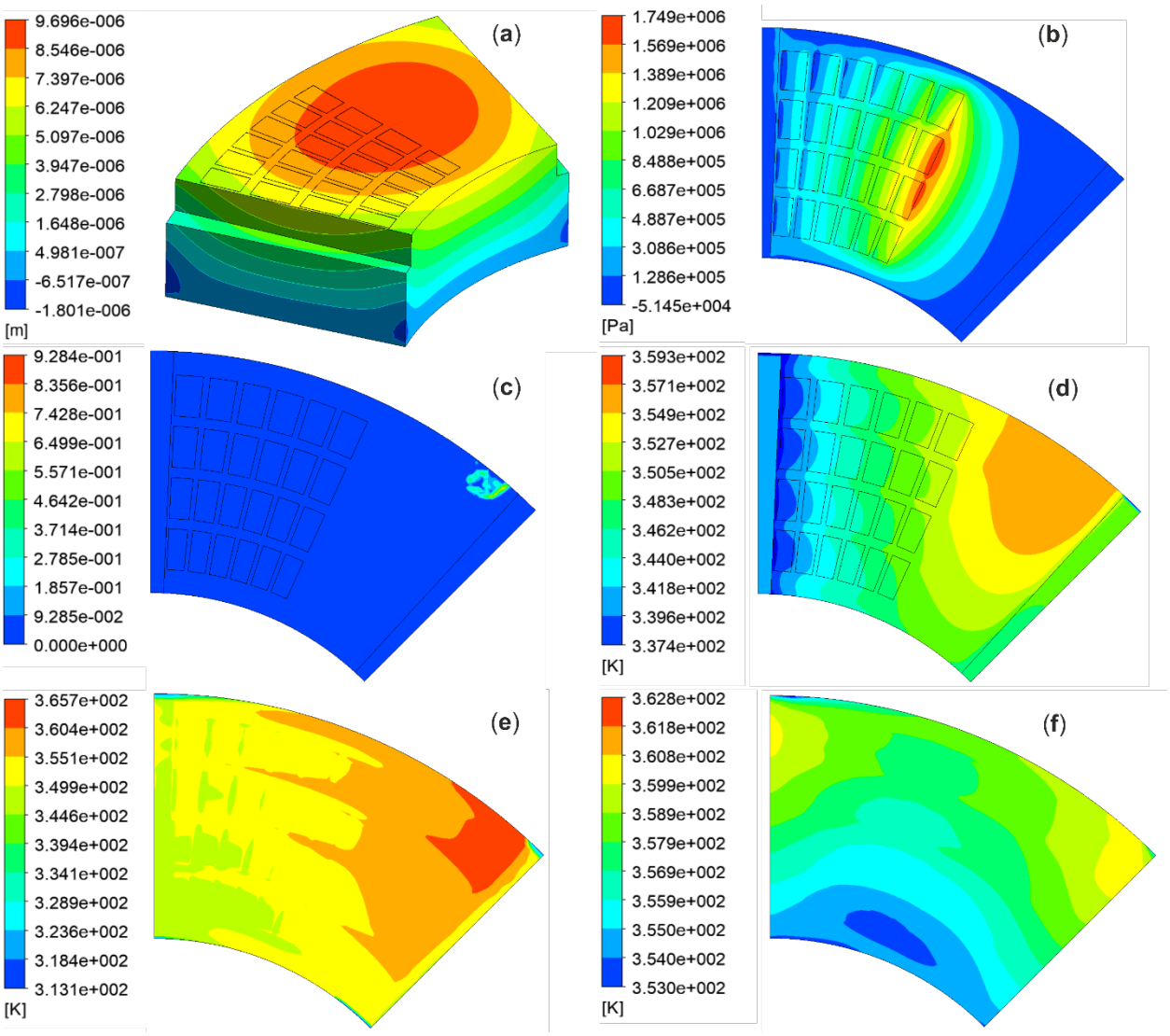

Figure 9 – (a) Z direction Mesh Displacement at the fluid/pad interface, (b) Pressure field at the fluid/pad interface, (c) Volume fraction field (blue: liquid oil, red: oil vapor) at the fluid/pad interface, Temperature field at: (d) the fluid/pad interface, (e) the midline of film thickness, and (f) the fluid/rotor Interface.

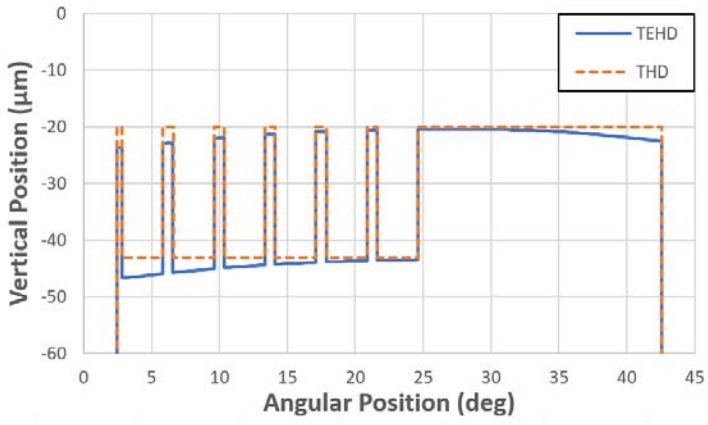

Figure 10 – Pad Geometries of the TEHD and THD models at a radius of 34m.

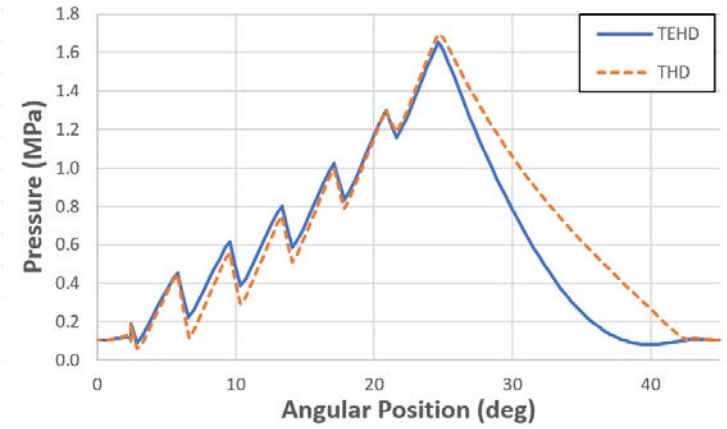

Figure 11 – Pressure Profiles of the TEHD and THD models at a radius of 34mm.

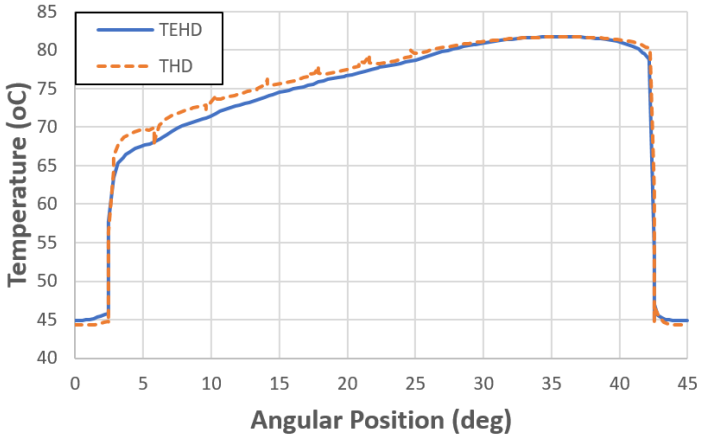

Figure 12 – Temperature Profiles of the TEHD and THD models at a radius of 34mm.

Table 8 – TEHD vs THD results comparison

	Units	THD	TEHD	Difference
Maximum Pressure	MPa	1.75	1.72	-1.7%
Load Carrying Capacity	N	278.2	242.6	-12.7%
Friction Torque	Nm	0.198	0.19	-4.0%
Coefficient of Friction	ul	0.0203	0.0224	+10.3%
Maximum Temperature	°C	92.7	89.5	-3.2
Maximum Volume Fraction	ul	92.8%	63.5%	-
Maximum Mesh Displacement	μm	-	9.7	-

To shed more light on the behavior of the pressure and temperature fields, 3D graphs of the pressure and temperature distributions at the fluid/pad interface have been generated for both the TEHD and THD models. Several pressure and temperature profiles were selected, for a wide range of radii in order to generate the 3D surface contours. In Fig. 13, it can be clearly observed that the pressure drop is steeper for the TEHD model in the outlet region. Moreover, in Fig. 13b the cavitation area for the TEHD model is highlighted. The decreased value of pressure bends the surface inwards in this region. In Fig. 14, a drop of the fluid temperature can be observed inside the dimples.

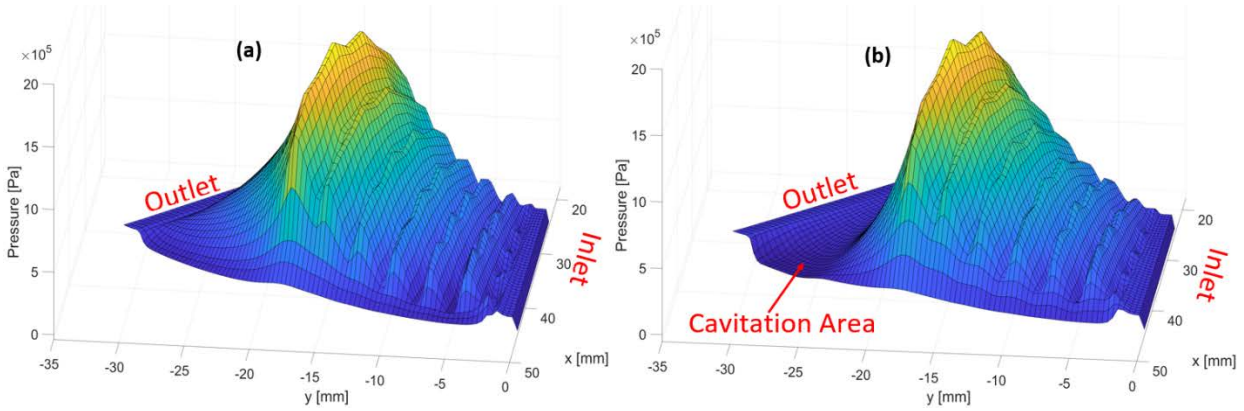

Figure 13 – 3-D pressure field at Fluid/Pad interface a) THD, b) TEHD

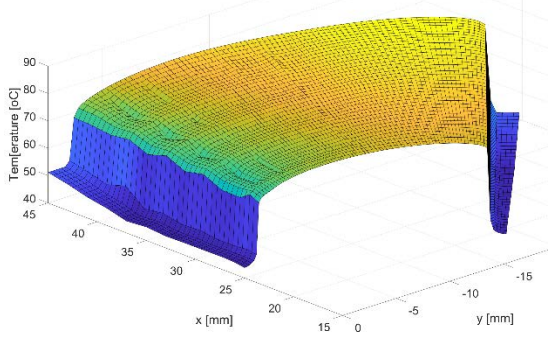

Figure 14 – 3-D temperature field at Fluid/Pad interface TEHD

TEHD Sensitivity Analysis

A sensitivity analysis of the design parameters has been performed utilising the TEHD model. A variation of ±2% for the textured length (L) and textured width (B) has been considered and ±2μm for the textured depth (TD). The results of the THD and TEHD optima are almost identical for the textured length and depth, as seen in Fig. 13. However, for a lower value of textured width there seems to be an increase of the LCC and a decrease of the friction torque, leading to an improvement of the coefficient of friction. In Fig. 13a the pad with the decreased texture width exhibits a larger maximum pressure area, which results in an increase of LCC by approximately 1%. The temperature of the fluid is slightly higher both at the fluid/pad and fluid/rotor interfaces for this design, as seen in Fig. 16c and Fig. 16e, which results in lower viscosity in this region and therefore to a decreased value of friction torque. The overall coefficient of friction is decreased by 1%. This indicates that bearing design optimisation with THD modeling is a valuable means for identifying optimal geometric design parameters of the bearing However, for accurate prediction of bearing performance, TEHD simulations should be performed.

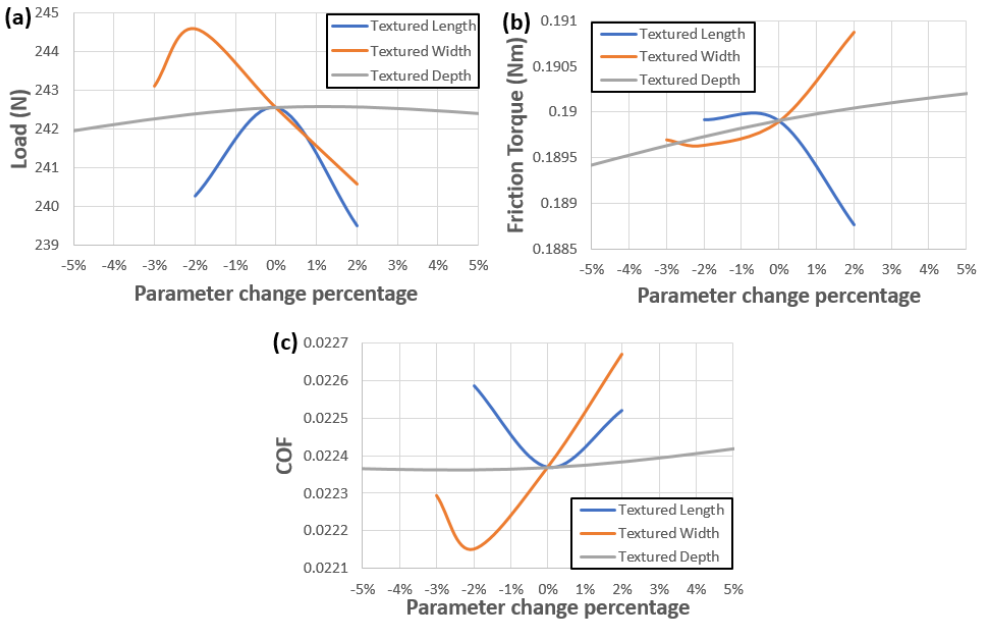

Figure 15 – TEHD Sensitivity analysis a) LCC, b) Friction torque c) Friction coefficient.

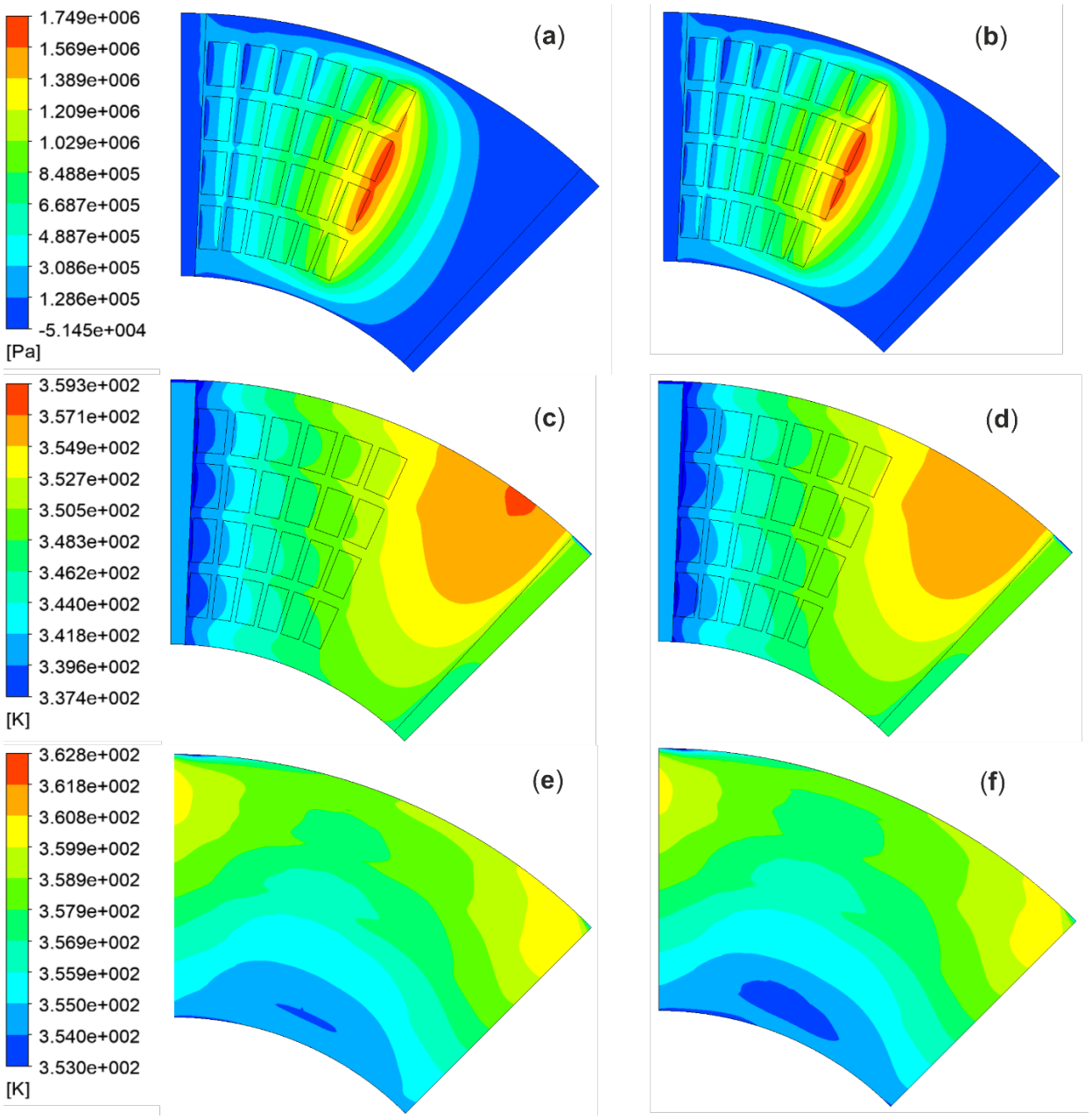

Figure 16 – Pressure field at the fluid/pad interface a) -2% of optimal Textured Width, b) THD optimal, Temperature field at the fluid/pad interface c)-2% of optimal Textured Width, d) THD optimal, Temperature field at the fluid/rotor interface e)-2% of optimal Textured Width, f) THD optimal

CONCLUSIONS

In the present work, a computational analysis of textured parallel thrust bearing has been performed. First, a thermohydrodynamic (THD) modelling approach has been used for optimising the texturing geometric parameters of the bearing, followed by a parametric analysis around the optimum, in order to validate the optimality of the obtained solution. Next, a thermoelastohydrodynamic (TEHD) modelling approach has been introduced, which takes into consideration the thermal and mechanical deformations of the pad geometry. TEHD utilises a 2-way FSI technique and has been used to re-evaluate the performance of the THD-optimal thrust bearing configuration. Finally, a sensitivity analysis of the textured geometry parameters with the TEHD model has been performed, in order to evaluate the optimality of the obtained solution with the new approach. The findings of the present study can be summarised as follows:

- The thermal deformation of the pad leads to a substantial alteration of the fluid geometry while generating a converging and a diverging region in the streamwise direction. The converging region extends from the leading edge (inflow) to the end of the textured surface area. This alteration enhances pressure build up on the inlet and hence decreases the cavitation probability within the dimples. Moreover, the converging geometry assists in increasing the inflow of cold lubricant into the pad, thus lowering considerably the overall temperature in the lubricant domain. On the other hand, the diverging region extends from the end of the textured surface area to the trailing edge (outflow). This leads to a substantial increase of the pressure drop in the outflow region, and therefore increases the cavitation probability at the outer radius of the trailing edge and decreases the load carrying capacity of the bearing.
- For a given value of the minimum film thickness, the TEHD simulation results demonstrated a reduction of load carrying capacity by 13% and of friction torque by 4%, leading to an increase of the coefficient of friction by 10%, in comparison to the THD simulation results. The above results point out that bearing thermal or mechanical deformations have a substantial effect on bearing performance, therefore they should be taken into consideration in the design stage of a high-performance bearings.

Based on the present study, a direct optimisation of the texture geometry parameters by a TEHD approach is extremely expensive computationally. The most realistic approach is an optimisation of the parameters with a THD-based analysis, and the fine-tuning of the geometry details and the quantification of performance indices by detailed TEHD simulations. These are essential for bearing applications which involve high rotational speeds, high thrust loads and high lubricating oil operating temperatures.

REFERENCES

[1] Rahmani R., Shirvan A., Shirvani H., 2007, 'Optimization of partially textured parallel thrust bearings with square-shaped micro-dimples', Tribology Transactions, Vol 50(3), pp. 401-406.

[2] Fu G., Untaroiu A., 2016, 'An Optimum Design Approach for Textured Thrust Bearing With Elliptical-Shape Dimples Using CFD and DOE Including Cavitation', ASME 2016 International Mechanical Engineering Congress and Exposition, Vol. 7, pp. 78-88.

[3] Brizmer V., Kligerman Y., Etsion I., 2003, "A Laser Surface Textured Parallel Thrust Bearing", Tribology Transactions, Vol. 46(3), pp. 397-403.

[4] Gropper D., Wang L., Harvey T., 2016, "Hydrodynamic lubrication of textured surfaces: A review of modeling techniques and key findings", Tribology International, Vol. 94, pp. 509-529.

[5] Papadopoulos C., Kaiktsis L., Fillon M., 2013, "Computational Fluid Dynamics Thermohydrodynamic Analysis of Three-Dimensional Sector-Pad Thrust Bearings with Rectangular Dimples", ASME Turbo Expo 2013: Turbine Technical Conference and Exposition, Vol. 7(B), pp. 30-40.

[6] Henry Y., Bouyer J., Fillon M., 2014, "An experimental analysis of the hydrodynamic contribution of textured thrust bearings during steady-state operation: A comparison with the untextured parallel surface configuration", Journal of Engineering Tribology, Vol 229, pp 362-375.

[7] X. Deng, C. Watson, M. He, R. Fittro, H. Wood, 2018, "Comparison of experimental, thermoelastohydrodynamic (TEHD) and thermal, non-deforming computational fluid dynamics (CFD) results for thrust bearings: part II", IMECE2018.

[8] E. J. Hahn and C. F. Kettleborough, 1968, "The Effects of Thermal Expansion in Infinitely Wide Slider Bearings—Free Thermal Expansion", J. of Lubrication Tech., Vol. 90, Issue 1, pp. 233-239.

[9] L. Dabrowski, M. Wasilczuk, 2004,"Evaluation of water turbine hydrodynamic thrust bearing performance on the basis of thermoelastohydrodynamic calculations and operational data", Proceedings of the Institution of Mechanical Engineers, Part J: Journal of Engineering Tribology, Vol. 218, Issue 5, pp. 413–421, https://doi.org/10.1243/1350650042128094.

[10] T. Brockett, L. Barrett, P. Allaire, 1996, "Thermoelastohydrodynamic Analysis of Fixed Geometry Thrust Bearings Including Runner Deformation", Tribology transactions, Vol. 39, Issue 3, pp. 555-562, DOI: 10.1080/10402009608983566.

[11] A. Tieu, 1986, "Thermo-Elasto-Hydrodynamic-Analysis of Step and Diaphragm Thrust Bearing", ASME. J. Tribol., Vol. 108, Issue 2, pp. 225–230, https://doi.org/10.1115/1.3261167.

[12] L. Zhai, Y. Luo, X Liu, F. Chen, Y. Xiao, Z. Wang, 2017, "Numerical simulations for the fluid-thermal-structural interaction lubrication in a tilting pad thrust bearing", Engineering Computations, Vol. 34, Issue 4, pp. 1149-1165, 10.1108/EC-08-2015-0209.

[13] G. Xu, F. Sadeghi, 1998, "A Thermal Elastohydrodynamic Lubricated Thrust Bearing Contact Model", International Compressor Engineering Conference, Paper 1226, https://docs.lib.purdue.edu/icec/1226.

[14] L. Dabrowski, M. Wasilczuk, 2004,"Evaluation of water turbine hydrodynamic thrust bearing performance on the basis of thermoelastohydrodynamic calculations and operational data", Proceedings of the Institution of Mechanical Engineers, Part J: Journal of Engineering Tribology, Vol. 218, Issue 5, pp. 413–421, https://doi.org/10.1243/1350650042128094

[15] L. Zhai, Y. Luo, X Liu, F. Chen, Y. Xiao, Z. Wang, 2017, "Numerical simulations for the fluid-thermal-structural interaction lubrication in a tilting pad thrust bearing", Engineering Computations, Vol. 34, Issue 4, pp. 1149-1165, 10.1108/EC-08-2015-0209.

[16] S. Glavatskih, M. Fillon, R. Larsson, 2001, "The Significance of Oil Thermal Properties on the Performance of a Tilting-Pad Thrust Bearing", Journal of Tribology, Vol. 124, Issue 2, pp. 377-385, https://doi.org/10.1115/1.1405129.

[17] S. Glavatskih, M. Fillon, 2004, "TEHD Analysis of Thrust Bearings With PTFE-Faced Pads", ASME/STLE 2004 International Joint Tribology Conference, Parts A and B, pp. 603-613, https://doi.org/10.1115/TRIB2004-64178.

[18] X. Lianga, X. Yana, W. Ouyanga, R. Woodd, Z. Liua, 2004, "Thermo-Elasto-Hydrodynamic analysis and optimization of rubbersupported water-lubricated thrust bearings with polymer coated pads", Journal of Tribology, Vol. 126, Issue 2, pp. 267-274, https://doi.org/10.1115/1.1645298.
[19] B. Kucinschi, K. DeWitt, M. Pascovici, 2004, "Thermoelastohydrodynamic (TEHD) Analysis of a Grooved Thrust Washer", Journal of Tribology, Vol. 126, Issue 2, pp. 267-274, https://doi.org/10.1115/1.1645298.
[20] M. Hartinger, M. Dumont, S. Ioannides, D. Gosman, H. Spikes, 2008, "CFD Modeling of a Thermal and Shear-Thinning Elastohydrodynamic Line Contact", Journal of Tribology, Vol. 130, Issue 4, https://doi.org/10.1115/1.2958077.
[21] A. Charitopoulos, D. Fouflias, C.I. Papadopoulos, L. Kaiktsis and M. Fillon, 2014, "Thermohydrodynamic analysis of a textured sector-pad thrust bearing: effects on mechanical deformations", Mechanics & Industry, Vol. 15, Issue 5, pp. 403-411.
[22] C. I. Papadopoulos, E. E. Efstathiou, P. G. Nikolakopoulos, L. Kaiktsis, 2011, "Geometry optimization of Textured Three-Dimensional Micro- Thrust Bearings", Journal of Tribology, Vol. 133, Issue 4, pp. 702-716.
[23] X. Jiang, J. Wang, J. Fang, 2011, "Thermal Elastohydrodynamic Lubrication Analysis of Tilting Pad Thrust Bearings", Proceedings of the Institution of Mechanical Engineers, Part J: Journal of Engineering Tribology, Vol. 225, Issue 2, pp. 51–57, https://doi.org/10.1177/2041305X10394408.
[24] A. Schenk, M. Ivantysynova, 2015, "A Transient Thermoelastohydrodynamic Lubrication Model for the Slipper/Swashplate in Axial Piston Machines", Journal of Tribology, Vol. 137, Issue 3, https://doi.org/10.1115/1.4029674.
[25] H. Tang, Y. Ren, J. Xiang, 2017, "A novel model for predicting thermoelastohydrodynamic lubrication characteristics of slipper pair in axial piston pump, International Journal of Mechanical Sciences, http://dx.doi.org/10.1016/j.ijmecsci.2017.03.010.
[26] A. Charitopoulos, M. Fillon, C. Papadopoulos, 2018, "Numerical investigation of parallel and quasi-parallel slider bearings operating underThermoElastoHydroDynamic (TEHD) regime", Tribology International, https://doi.org/10.1016/j.triboint.2018.12.017.
[27] ANSYS, Inc. 2011, ANSYS CFX-Solver Theory Guide. http://read.pudn.com/downloads500/ebook/2077964/cfx_thry.pdf.

NOMENCLATURE

H_{min}:	Minimum film thickness (μm)
V:	velocity vector (m/s)
p:	the static pressure (Pa)
T:	the temperature (K)
τ:	the viscous stress tensor
ρ:	the oil density (kg/m^3)
μ:	the oil dynamic viscosity (kg/(m*s))
Φ	heat generated by internal fluid friction (J)
c_{pf}:	oil specific heat capacity (J/(kg*K))
λ_f:	oil thermal conductivity (W/(m*K))
λ_{sp}:	pad thermal conductivity (W/(m*K))
λ_{sr}:	rotor thermal conductivity (W/(m*K))
σ	stress vector
[D]:	elasticity matrix
$\{\varepsilon^{el}\}$:	elastic strain vector
$\{\varepsilon\}$:	total strain vector
$\{\varepsilon^{th}\}$:	thermal strain vector
α^{se}:	secant coefficient of thermal expansion
σ_B	is the surface tension coefficient
R_B	bubble radius
T_L	Length of the texture cell
T_B	Breadth of the texture cell